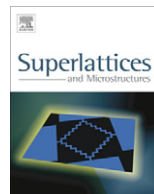




ELSEVIER

Contents lists available at ScienceDirect

Superlattices and Microstructures

journal homepage: www.elsevier.com/locate/superlattices

Stiffness properties of porous silicon nanowires fabricated by electrochemical and laser-induced etching

Khalid Omar^a, Y. Al-Douri^{b,*}, Asmiet Ramizy^a, Z. Hassan^a

^a Nano-Optoelectronics Research and Technology Laboratory, School of Physics, Universiti Sains Malaysia, 11800 Penang, Malaysia

^b Institute of Nano Electronics Engineering, University Malaysia Perlis, Kangar, Perlis, Malaysia

ARTICLE INFO

Article history:

Received 14 April 2011

Accepted 18 May 2011

Available online 25 May 2011

Keywords:

Nanowire

Stiffness

Elasticity

Laser-induced etching

Chemical etching

ABSTRACT

Nanowires with dimensions of few nanometers were formed on the whole etched surface. The optical analysis of silicon nanostructures was studied. Blue shift luminescence was observed at 660 nm for PS produced by electrochemical etching, and at 629 nm for laser-induced etching. PS produced a blue shift at 622 nm using both etching procedures simultaneously. X-ray diffraction (XRD) was used to investigate the crystallites size of PS as well as to provide an estimate of the degree of crystallinity of the etched sample. Refractive index, optical dielectric constant, bulk modulus and elasticity are calculated to investigate the optical and stiffness properties of PS nanowires, respectively. The elastic constants and the short-range force constants of PS are investigated.

© 2011 Elsevier Ltd. All rights reserved.

1. Introduction

The nanoparticles, nanowires, nanobelts and nanotubes are attractive because of their unique chemical, physical and electrical properties compared to the bulk form of the corresponding material. Single electron transistors, single-electron memory arrays, precise size definition and location of nanostructured semiconductor materials are considered vital to obtain good device performance [1–4].

The characteristics of the surface strongly affect the properties of Si. Therefore, the quantum confinement effects are considered to control the mechanism of the luminescence in nanocrystallites [5,6]. The reduction of size to a few nanometers is required to observe efficient light emission as it modifies in the electronic, optical and vibration properties [7].

Recently, Lin et al. [8] prepared vertical and single crystalline porous silicon nanowire (SiNW) arrays using the silver-assisted electroless etching method. They used the selenization treatment at

* Corresponding author. Tel.: +60 4 9775021; fax: +60 4 9798578.

E-mail address: yaldouri@yahoo.com (Y. Al-Douri).

700 °C and found it is useful for investigating the photoluminescence (PL) properties of porous SiNWs. Also, they observed PL peaks blue-shift to 650 nm. They proved that the selenization treatment could increase the absorbance of the SiNWs and also enhance the stability of the PL intensity which it is useful as nanoscale optoelectronic devices. Silicon nanowire (SiNW) arrays of smooth surface by using a low-cost and facile Ag-assisted chemical etching technique and found experimentally that the reflectance can be significantly suppressed (<1%) over a wide solar spectrum (300–1000 nm) in the as-grown samples are successfully fabricated by Xie et al. [9]. They obtained from further simulation study on the light absorption in SiNW arrays, a photocurrent enhancement of up to 425% per unit volume of material as compared to crystalline Si. In addition, they have demonstrated experimentally and theoretically that the as-grown samples have an omnidirectional high-efficiency antireflection property. Also, Ozdemir et al. [10] have been fabricated vertically aligned silicon nanowire (SiNW) arrays over large areas using an electroless etching (EE) method, which involves etching of silicon wafers in a silver nitrate and hydrofluoric acid based solution. They analyzed Si NW arrays using field emission scanning electron microscope (FE-SEM), studied a linear dependency of nanowire length to both temperature and time and showed the change in the growth rate of Si NWs at increased etching durations. Furthermore, they investigated the effects of EE parameters on the optical reflectivity of the SiNWs.

One of the porous silicon (PS) fabrication methods [11–15] is to electrochemically etch bulk Si wafers in an electrolyte solution [14,15]. This structure is mechanically fragile and unstable with oxidation, alternatively. Porous silicon micro column array can be created by exposing the Si substrate to a powerful laser source [11–15]. This formation cannot be repeated if the laser power is insufficient to melt the Si surface.

The objective of this study is to investigate the refractive index using specific models, optical dielectric constant, stiffness, elasticity and short-range force constants of PS nanowires.

2. Practical procedure

Porous silicon was fabricated by electrochemical etching of n-type Silicon wafer with (1 1 1) orientation, resistivity of 0.75 Ω .cm, and thickness of 283 μ m. The wafer was placed in an electrolyte solution (hydrofluoric acid (HF): ethanol in the ratio of 10 ml: 40 ml) with current density of 100 mA/cm² for about 30 min. Before etching process, the Si substrate was cleaned to remove the oxide layer by the Radio Corporation of America (RCA) method. The Si wafer was immersed in HF acid to remove the native oxide. The electrochemical cell was made of Teflon and has a circular aperture on its bottom under which the silicon wafer was sealed. The cell was a two-electrode system with a silicon wafer as an anode and platinum as a cathode. The process was carried out at room temperature.

After etching process, all the samples were rinsed with ethanol and dried in the air. Laser-Induced Etching (LIE) was done by using Continuous Wavelength (CW) laser diode beam ($\lambda = 635$ nm, 1.95 eV) at 1 mm diameter without using any electrodes as normally carried out in the traditional methods of etching. The rinsed samples were placed in an electrolyte solution with HF concentration of 40% with laser power density of 51 W/cm² and irradiation time of 2 h at room temperature. Photoluminescence (PL) measurement was also performed at room temperature by using He–Cd laser ($\lambda = 325$ nm) [16].

3. Results and discussion

3.1. Photoluminescence spectroscopy

Fig. 1 shows the PL spectrum at room temperature for the PS prepared by two etching techniques. PL spectra were measured with laser excitation photon energy of 3.81 eV. Blue shift luminescence was observed at 660 nm with Full-Width and Half Maximum FWHM of 135 nm (9.18 eV) for the PS produced by electrochemical etching and at 629 nm with FWHM of 110 nm (11.27 eV) for laser-induced etching. The PS fabricated by using both etching procedures simultaneously produced a blue shift at 622 nm with FWHM of 106 nm (11.6 eV). The energy gap of PS increases to 1.87, 1.97, and 1.99 eV for electrochemical, laser-induced and integrated etching procedures, respectively [16]. Broadening of the

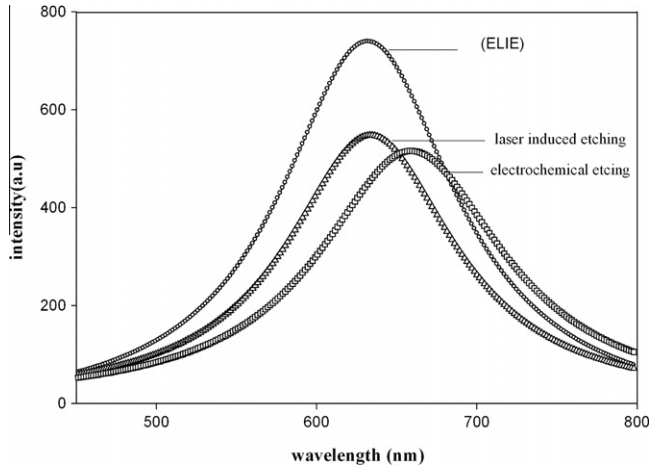


Fig. 1. PL spectra of PS using electrochemical, laser-induced and integrated etching techniques.

band gap energy occurs when there is a decrease in the crystallite size [17]. An estimate of the size of the Si nanocrystallite was identified using the effective mass theory. Assuming that infinite potential barriers, the E_g of the 3D confined Si were obtained as [18].

$$E_n(\text{eV}) = E_g + \frac{\hbar^2}{8d^2} \left(\frac{1}{m_e^*} + \frac{1}{m_h^*} \right), \quad (1)$$

where E_g is the bulk silicon energy gap, d is the diameter of the spherical particle and m_e^* , m_h^* represent the electron and hole effective mass, respectively (at 300 K, $m_e^* = 0.19m_0$, $m_h^* = 0.16m_0$ and $E_g = 1.12$ eV) [19]. From Eq. (1), the obtained radiuses of the nanocrystallites E_n were 5, 4.2, and 4 nm for the three techniques respectively. The reduction of dimension to nanometer sizes leads to a change in the physical properties of Si drastically. This is attributed to the charge carrier quantum confinement. This means that the particles are confined in the lower dimension and the probability of the recombination of the electrons and holes is higher in low dimensional structure. This leads to high emission efficiency from high porosity structures arising from the quantum confinement effects as a result of the conversion of the material's energy gap from indirect to direct band gap. The change from indirect to direct band gap occurs when the nanostructures form and the transition are dominated by porosities, surface passivation, pore size and size distribution [20].

The photoluminescence intensity at room temperature shows an increasing trend with laser power density. This strength of photoluminescence output becomes stronger when the porosity increases. This means the intensity of photoluminescence is proportional to the number of emitted photons on the porous surface. This surface experiences shrinking of the size caused by deeper etching which in turn leads to increase in the number of transitions inside the structure. This leads to increase in PL intensity.

3.2. Optical properties

The refractive index n is an important physical parameter related to microscopic atomic interactions. Theoretically, the two different approaches in viewing this subject are the refractive index related to density, and the local polarizability of these entities [21].

On the other hand, the crystalline structure represented by a delocalized picture, n will be closely related to the energy band structure of the material, complicated quantum mechanical analysis requirements and the obtained results. Many attempts have been made to relate the refractive index and the energy gap E_g through simple relationships [22–27].

However, these relationships of n are independent of temperature and incident photon energy. Here, the various relationships between n and E_g will be reviewed. Ravindra et al. [27] suggested different relationships between the band gap and the high frequency refractive index and presented a linear form of n as a function of E_g :

$$n = \alpha + \beta E_g, \quad (2)$$

where $\alpha = 4.048$ and $\beta = -0.62 \text{ eV}^{-1}$.

To be inspired by simple physics of light refraction and dispersion, Herve and Vandamme [28] proposed an empirical relation as:

$$n = \sqrt{1 + \left(\frac{A}{E_g + B}\right)^2}, \quad (3)$$

where $A = 13.6 \text{ eV}$ and $B = 3.4 \text{ eV}$. Ghosh et al. [29] took a different approach to the problem by considering the band structural and quantum-dielectric formulations of Penn [30] and Van Vechten [31]. Introducing A as the contribution from the valence electrons and B as a constant additive to the lowest band gap E_g , the expression for the high-frequency refractive index is written as:

$$n^2 - 1 = \frac{A}{(E_g + B)^2}, \quad (4)$$

where $A = 25E_g + 212$, $B = 0.21E_g + 4.25$ and $(E_g + B)$ refers to an appropriate average energy gap of the material. Thus, these three models of variation n with energy gap have been calculated. The calculated refractive indices of the end-point compounds are calculated in Table 1. The optical dielectric constant ϵ_∞ is calculated using $\epsilon_\infty = n^2$ [33] and depends on the refractive index. In Table 1, the calculated values of ϵ_∞ using the three models are investigated for different etching techniques. As with Ravindra et al. [27], this is more appropriate for studying solar cell optical properties.

3.3. X-ray diffraction

XRD was used to investigate the size of the crystallites of the PS and to estimate the crystalline degree of etched sample. Fig. 2a shows a very sharp peak at $2\theta = 28.46^\circ$ for the Si as grown sample. Fig. 2b and c shows a small broadening peak of the PS when laser power density and irradiation time gradually increase. Fig. 2d shows broadening in a spectrum at power density of 51 W/cm^2 with average diameter of crystallites of 13 nm . The two different etching techniques used in this study are to obtain different diffraction angles of different shapes on the porous layers [16]. Many types of porosity were provided to investigate if there is matching between the theoretical part and experimental part which helps to calculate the grain size. The average grain size (crystallite size) corresponds to the average diameter (t) of the crystallite columns which can be calculated by using Debye–Scherrer formula as shown in Eq. (5).

$$t = \frac{0.9\lambda}{B_2 \cos \theta}, \quad (5)$$

Table 1

Calculated refractive using indices Ravindra et al. [27], Herve and Vandamme [28], and Ghosh et al. [29] models compared with others corresponding to optical dielectric constant for PS of different etching techniques.

Etching techniques	n	ϵ_∞
Electrochemical etching	2.88 ^a 2.76 ^b 2.66 ^c 3.88 ^d	11.22 ^a 8.46 ^b 8.35 ^c 11.68 ^d
Laser-induced etching	2.82 ^a 2.72 ^b 2.63 ^c	10.04 ^a 7.78 ^b 7.67 ^c
Electrochemical and laser-induced etching	2.81 ^a 2.71 ^b 2.62 ^c	8.64 ^a 7.18 ^b 7.07 ^c

^a Ref. [27].

^b Ref. [28].

^c Ref. [29].

^d Ref. [32] expt.

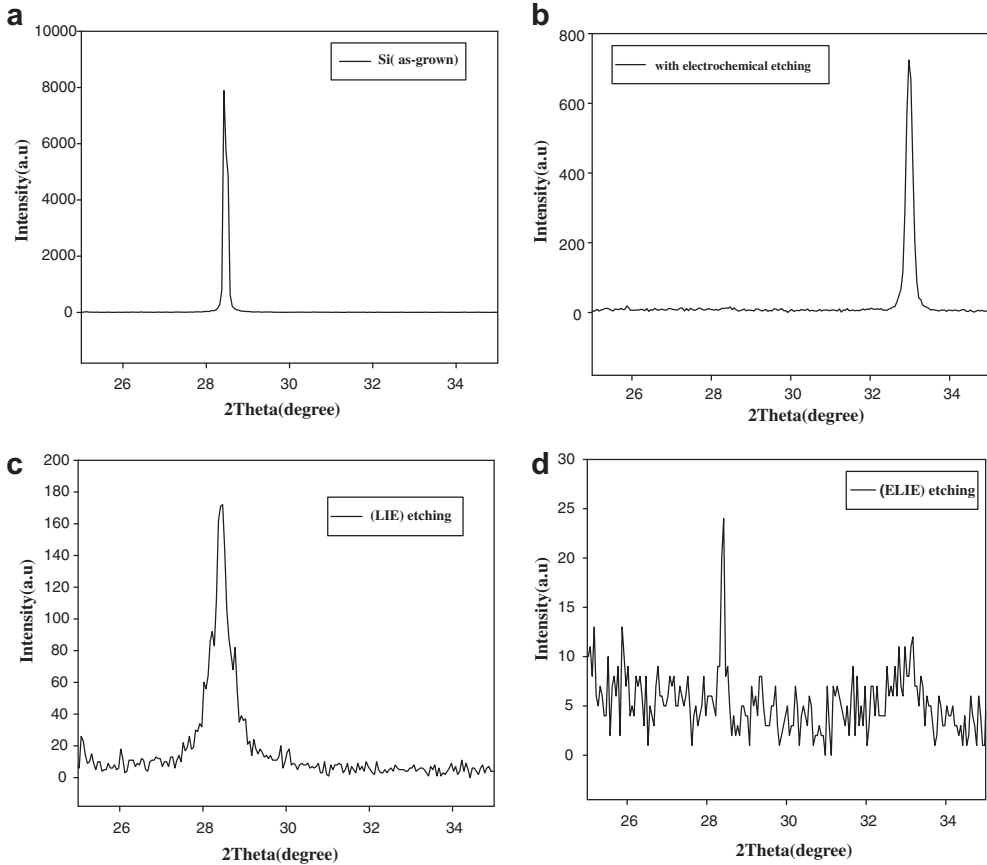


Fig. 2. X-ray diffraction of PS prepared by (a) As grown, (b) Electrochemical etching, (c) Laser-induced etching and (d) Integrated etching procedures.

where $B_{\frac{1}{2}}$ is the full width at half maximum of the diffraction peak, θ is the diffraction angle, and λ is 1.54 \AA of the Cu $K\alpha$ line. The crystallite size reduced through these measurements showed a variation from 13 to 6 nm via electrochemical and laser etching rad. The decrease in the average of the crystallite size indicated that there is an increase in the porosity [34,35]. In addition, the reduction in the crystallite size can be inferred through the increase in broadening of the XRD spectra. On the other hand, to select the best etching technique which may be used to fabricate the optoelectronics devices as a high quality substrate or as a buffer layer, the average discrepancy% between the PS lattice constant and the bulk silicon lattice constant was calculated by using Eq. (6).

$$\Delta D = \frac{a_{ps} - a_{bs}}{a_{bs}} \times 100\%, \quad (6)$$

where a_{ps} is porous silicon lattice constant and a_{bs} is bulk silicon lattice constant.

For diamond structure of silicon, the lattice constant was considered as a function of the interplanar spacing d_{hkl} by using Eq. (6) [36]

$$a = d_{hkl} \sqrt{h^2 + k^2 + l^2}, \quad (7)$$

where hkl are Miller indices.

Table 2 shows that discrepancy is –13.2% for the electrochemical etching, 0.11% for the laser-induced etching and 0.36% for the fabricated sample by using integrated etching. This means that the laser induced etching is a more suitable technique which may be used to fabricate the optoelectronic devices such as PS solar cell and PS gas sensors.

3.4. Bulk modulus

It is known that the bulk modulus is a reflectance of the materials stiffness that it is important in different industries. Many authors [37–42] have made various efforts to explore thermodynamic properties of solids. In these studies, authors have examined the thermodynamic properties such as the inter-atomic separation and the bulk modulus of solids with different approximations and best-fit relations [39–42]. It has become possible to compute with great accuracy an important number of structural and electronic properties of solids. The *ab initio* calculations are complex and require significant effort. Therefore, more empirical approaches have been developed [43,44] to compute properties of materials. In many cases, the empirical methods offer the advantage of applicability to a broad class of materials and to illustrate trends. In many applications, these empirical approaches do not give highly accurate results for each specific material, but are still very useful. Cohen [45] has established an empirical formula for calculation of the bulk modulus B_0 ; based on the nearest-neighbor distance. His result is in agreement with experimental values. Lam et al. [46] have derived an analytical expression for the bulk modulus from the total energy. This expression is different in structure from the empirical formula but gives similar numerical results. Also, they have obtained an analytical expression for the pressure derivative B_0 of the bulk modulus. Our group [47] used a concept based on the lattice constant to establish an empirical formula for the calculation of the bulk modulus. The results are in good agreement with experimental data and other calculations. The theory yields a formula with two attractive features. Only the lattice constant is required as input, the computation of B_0 itself is trivial. Consideration of hypothetical structure and simulation of the experimental conditions are required to make practical use of this formula.

The aim is to see how a qualitative concept, such as the bulk modulus, can be related to the lattice constant. It was argued that the dominant effect is the degree of covalency characterized by Phillips' homopolar gap E_h [43], and one reason for presenting these data in this work is that the validity of our calculations that is not restricted in computed space. We thus believe that the data will prove valuable for future work in this field.

An important reason for studying B_0 is the observation of clear differences between the lattice constant for PS using different techniques as seen in Table 2.

The basis of our model is the lattice constant as seen in Table 2. Fitting of these data gives the following empirical formula [47]:

$$B_0 = [3000 - 100\lambda] \left(\frac{a}{2}\right)^{-3.5}, \quad (8)$$

where a is the lattice constant (in Å) and λ is an empirical parameter which accounts for the effect of ionicity; $\lambda = 0; 1, 2$ for group IV, III–V, and II–VI semiconductors, respectively. In Table 3, the calculated bulk modulus values are compared with experimental values and results of Cohen [45], Lam et al. [46] and Al-Douri et al. [48,49].

We may conclude that the present bulk moduli calculated in a different way than the definition of Cohen are in accord with the experimental value, and exhibit the same chemical trends as those found

Table 2

The discrepancy between bulk Si and PS using different etching techniques.

Etching techniques	a_{ps} (Å)	a_{bs} (Å)	Discrepancy ΔD (%)
Electrochemical etching	4.70	5.42	–13.2
Laser-induced etching	5.43	5.42	0.11
Electrochemical and laser-induced etching	5.44	5.42	0.36

Table 3

Calculated bulk modulus, elastic constants and short-range force constants for PS of etching techniques along with Cohen [45], Lam et al. [46], Al-Douri et al. [48,49] and experimental data [45,52]. The experimental values are for bulk Si.

Etching techniques	B_0 (GPa)	B_0 (GPa)	B_0 (GPa)	C_{11} (10^{11} dyn/ cm ²)	C_{12} (10^{11} dyn/ cm ²)	C_{44} (10^{11} dyn/ cm ²)	α (N/ m)	α (N/ m)
Electrochemical etching	150.7 [*]	98 ^a	98 ^b 100 ^c 100.7 ^d 100.9 ^e	13.27 [*] 16.57 ^f	8.65 [*] 6.39 ^f	8.99 [*] 7.96 ^f	46.83 [*] 48.50 ^f	5.51 [*] 13.81 ^f
Laser-induced etching	90.9 [*]			6.390 [*]	2.74 [*]	7.77 [*]	20.19 [*]	9.19 [*]
Electrochemical and laser-induced etching	90.39 [*]			6.393 [*]	2.68 [*]	7.74 [*]	20.03 [*]	9.31 [*]

^{*} Calculated value.

^a Ref. [48] expt.

^b Ref. [48].

^c Ref. [49].

^d Ref. [50].

^e Ref. [51].

^f Ref. [52] expt.

for the values derived from the experimental value as seen in Table 3. Our calculations results using laser induced etching are in good agreement with experiment, Cohen [45], Lam et al. [46] and our previous works [48,49], that regard a very suitable technique for fabricating different optoelectronic devices.

We now turn our attention to the elastic properties. In this respect, the elastic constants namely C_{11} , C_{12} and C_{44} have been calculated following the same procedure used by Al-Douri et al. [32] that was based essentially on the work of Baranowski [50], where C_{11} , C_{12} and C_{44} are expressed as,

$$C_{11} = \frac{\sqrt{3}h^2}{4d^5m} (1 - \alpha_p^2)^{\frac{1}{2}} \left[4.37(5 + \lambda)(1 - \alpha_p^2) - 0.6075 \right], \quad (9)$$

$$C_{12} = \frac{\sqrt{3}h^2}{4d^5m} (1 - \alpha_p^2)^{\frac{1}{2}} \left[4.37(3 - \lambda)(1 - \alpha_p^2) + 0.6075 \right], \quad (10)$$

$$C_{44} = \frac{\sqrt{3}}{4d} (\alpha + \beta) - 0.136 SC_0 - C\xi^2, \quad (11)$$

In Eqs. (9)–(11), d is the nearest neighbor distance, λ is a dimensionless parameter which has a constant value of 0.738 [50] and m is the electron mass. The quantities α and β in Eq. (11) are the short-range force constants. They represent the bond-stretching and bond-bending force constants, respectively and are expressed as [51],

$$\alpha = \frac{d}{\sqrt{3}} (C_{11} + 3C_{12}) + \frac{d}{3\sqrt{3}} (1.473 SC_0), \quad (12)$$

$$\beta = \frac{d}{\sqrt{3}} [(C_{11} - C_{12}) - 0.053 SC_0], \quad (13)$$

The parameter ξ is the internal-strain parameter. The quantities S and C_0 are obtained using the following expressions,

$$S = \frac{Z^*2}{\varepsilon(0)}, \quad (14)$$

$$C_0 = \frac{e^2}{d^4}, \quad (15)$$

S is an effective charge parameter, C_0 has the dimensions of an elastic constant and z^* is the effective charge. More details about the determination of the quantities C , ξ and z^* are given in Ref. [51]. $\epsilon(0)$ is the static dielectric constant.

Our results concerning C_{11} , C_{12} and C_{44} of different etching techniques for PS are given in Table 3 including the experimental data for comparison. Generally, our results agree reasonably well with those reported in the literature. Qualitatively, the trends of elastic constants of PS are similar. From the quantitative point of view, the elastic constants show considerable differences according to different etching techniques. The calculated bond-stretching α and bond-bending β force constants of PS for different etching techniques are shown in Table 3. From Table 3, one can see that our results agree well with those obtained experimentally [52]. It is confirmed that the laser induced etching is the recommended technique for high technological applications due to it blows average results between hardness and suppleness fit to solar cells.

4. Conclusion

Simultaneous electrochemical and laser-induced etching processes were used to synthesize nanowires. The efficiency of high emission from high porosity structures was created via quantum confinement effect as a result of change in the band gap from indirect to direct. The obtained PS nanowire results of optical, structural, elastic and force constants recommend that laser induced etching is more suitable technique and Ravindra et al. is more appropriate model for fabrication the optoelectronic devices such as PS solar cells and PS gas sensors.

This porous surface proved to be an excellent antireflection coating for the incident light compared with other etching techniques. This means that this technique has promising great control over the resultant PS nanostructure. The reduction in the crystallite size was confirmed through broadening of the FWHM obtained from the XRD spectra.

Acknowledgments

The authors would like to acknowledge the support of Universiti Sains Malaysia. One of us, (Y. A.) would like to acknowledge the financial support presented by FRGS grants numbered: 9003-00249 & 9003-00255, and TWAS-Italy for the full support of his visit to JUST-Jordan under TWAS-UNESCO Associateship.

References

- [1] B. Voigtl, M. Kawamura, V. Cherepanov, *J. Phys. Condens. Mater.* 16 (2004) 1535.
- [2] S. Tekada, K. Ishino, Y. Inoue, A. Ishida, *Jpn. J. Appl. Phys.* 44 (2005) 5664.
- [3] H. Lohmeyer, C. Kruse, K. Sebald, J. Gutowski, D. Hommel, *Appl. Phys. Lett.* 89 (2006) 1107.
- [4] J. Robert, L. Jan, *Microelectron. Eng.* 61–62 (2002) 563.
- [5] M. Voos, Ph. Uzan, C. Delalande, G. Bastard, *Appl. Phys. Lett.* 61 (1992) 1213.
- [6] S.M. Prokes, J.A. Freitas Jr., P.C. Searson, *Appl. Phys. Lett.* 60 (1992) 3295.
- [7] R.L. Smith, S.D. Colline, *J. Appl. Phys.* 71 (1992) R1.
- [8] L. Lin, X. Sun, R. Tao, J. Feng, Z. Zhang, *Nanotechnology* 22 (2011) 075203.
- [9] W.Q. Xie, J.I. Oh, W.Z. Shen, *Nanotechnology* 22 (2011) 065704.
- [10] B. Ozdemir, M. Kulakci, R. Turan, H.E. Unalan, *Nanotechnology* 22 (2011) 155606.
- [11] Y. Chen, A. Vertes, *Anal. Chem.* 78 (2006) 5835.
- [12] J.D. Cuiffi, Dj. Hayes, S.J. Fonash, K.N. Brown, A.D. Jones, *Anal. Chem.* 73 (2001) 1292.
- [13] E.V. Astrova, T.N. Borovinskaya, A.V. Tkachenko, S. Balakrishnan, T.S. Perova, A. Rafferty, Y.K. Gun'ko, *J. Micromech. Microeng.* 14 (2004) 1022.
- [14] S. Tuomikoski, K. Huikko, K. Grigoras, P. Ostman, R. Kostianinen, M. Baumann, J. Abian, T. Kotiaho, S. Franssila, *Lab. A Chip* 2 (2002) 247.
- [15] V.V. Doan, R.M. Penner, M.J. Sailor, *J. Phys. Chem.* 97 (1993) 4505.
- [16] A. Ramizy, Z. Hassan, Kh. Omar, *J. Mater. Sci.: Mater. Electron.* (2011). doi:10.1007/s10854-010-0199-3.
- [17] O.M. Khalid, N. Ali, Z. Hassan, M. Hashim, H. Abu Hassan, *J. Optoelectron. Advan. Mater.* 10 (2008) 2653.
- [18] S. Ossicini, L. Pavesi, F. Priolo, *Light Emitting Silicon for Microphotonics*, in: A. Fujimori et al. (Eds.), Springer Tracts in Modern Physics, Springer, Berlin, 2003.
- [19] S.M. Sze, K.K. Ng, *Physics of Semiconductor Devices*, John Wiley & Sons, New Jersey, 2003.
- [20] L.H. Lin, D.X. Li, J.Y. Feng, *Nanoscale Res. Lett.* 4 (2009) 409.
- [21] N.M. Balzaretti, J.A.H. da Jornada, *Solid State Commun.* 99 (1996) 943.

- [22] T.S. Moss, Proc. Phys. Soc. B 63 (1950) 67.
- [23] V.P. Gupta, N.M. Ravindra, Phys. Stat. Sol. B 100 (1980) 715.
- [24] Y. Al-Douri, Mater. Chem. Phys. 82 (2003) 49.
- [25] Y. Al-Douri, Y.P. Feng, A.C.H. Huan, Solid State Commun. 148 (2008) 521.
- [26] P. Hervé, L.K.J. Vandamme, Infrared Phys. Technol. 35 (1994) 609.
- [27] N.M. Ravindra, S. Auluck, V.K. Srivastava, Phys. Stat. Sol. (b) 93 (1979) K155.
- [28] P.J.L. Herve, L.K.J. Vandamme, J. Appl. Phys. 77 (1995) 5476.
- [29] D.K. Ghosh, L.K. Samanta, G.C. Bhar, Infrared Phys. 24 (1984) 34.
- [30] D.R. Penn, Phys. Rev. 128 (1962) 2093.
- [31] J.A. Van Vechten, Phys. Rev. 182 (1969) 891.
- [32] Y. Al-Douri, N.M. Ahmed, N. Bouarissa, A. Bouhemadou, Mater. Design. (2011), doi:10.1016/j.matdes.2011.03.010.
- [33] G.A. Samara, Phys. Rev. B 27 (1983) 3494.
- [34] S.V. Bhoraskar, T. Bhave, T.A. Railkar, Bull. Mater. Sci. 17 (1994) 523.
- [35] J.J. Yon, K. Barla, R. Herino, G.J. Bomchitl, J. Appl. Phys. 62 (1987) 1042.
- [36] P.F. Fewster, X-ray Scattering Form Semiconductors, World Scientific Publishing, USA, 2003.
- [37] A.M. Sherry, M. Kumar, J. Phys. Chem. Solids 52 (1991) 1145.
- [38] J.L. Tallon, J. Phys. Chem. Solids 41 (1980) 837.
- [39] M. Kumar, S.P. Upadhyaya, Phys. Stat. Sol. (b) 181 (1994) 55.
- [40] M. Kumar, Physica B 205 (1995) 175.
- [41] R.K. Pandey, J. Phys. Chem. Solids 59 (1998) 1157.
- [42] Q. He, Z-T. Yan, Phys. Stat. Sol. (b) 223 (2001) 767.
- [43] J.C. Phillips, Bonds and Bands in Semiconductors, Academic Press, San Diego, 1973.
- [44] W.A. Harison, Electronic Structure and the Properties of Solids, General Publishing Company, Toronto, 1989.
- [45] M.L. Cohen, Phys. Rev. B 32 (1985) 7988.
- [46] P.K. Lam, M.L. Cohen, G. Martinez, Phys. Rev. B 35 (1987) 9190.
- [47] Y. Al-Douri, H. Abid, H. Aourag, Mater. Chem. Phys. 87 (2004) 14.
- [48] Y. Al-Douri, H. Abid, H. Aourag, Physica B 322 (2002) 179.
- [49] Y. Al-Douri, Res. Lett. Mater. Sci. 2007 (2007) 57143.
- [50] J.M. Baranowski, J. Phys. C 17 (1984) 6287.
- [51] N. Bouarissa, R. Bachiri, Physica B 322 (2002) 193.
- [52] R.M. Martin, Phys. Rev. B 1 (1970) 4005.